Research Article

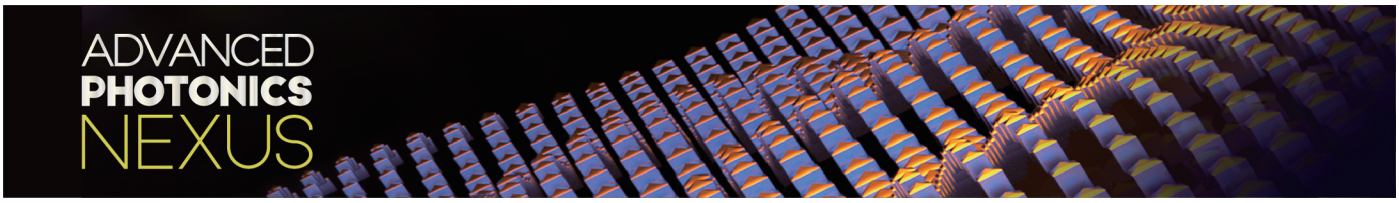

Er^{3+}-Yb^{3+}-Tm^{3+} tri-doped La_2O_3-Al_2O_3 glasses for low-power-consumption ultrawideband on-chip optical waveguide amplifiers

Zhengkai Li,[a] Mingjie Zhang,[b,*] Yuanzhi Chen,[a,c,*] Junchang Lu,[b] Zhanbo Wen,[b] Banghu Wei,[b] Mengyi Wang,[a] Jiayue Xu,[a] and Qingli Zhang[d]

[a]Shanghai Institute of Technology, School of Material Science and Engineering, Shanghai, China
[b]Jinan University, College of Physics and Optoelectronic Engineering, Guangzhou, China
[c]Nanyang Technological University, School of Electrical and Electronic Engineering, Singapore, Singapore
[d]Chinese Academy of Sciences, Anhui Institute of Optics and Fine Mechanics, Hefei, China

Abstract. In the field of short-range optical interconnects, the development of low-power-consumption, ultrawideband on-chip optical waveguide amplifiers is of critical importance. Central to this advancement is the creation of host materials that require low pump power and provide ultrabroadband emission capabilities. We introduce a tri-doped lanthanum aluminate glass (composition: $5Er_2O_3$-$5Yb_2O_3$-$0.2Tm_2O_3$-$43.8La_2O_3$-$46Al_2O_3$), which exhibits exceptional near-infrared (NIR) luminescence intensity, significantly outperforming other bands by 3 orders of magnitude. This glass can achieve an ultrawideband NIR gain spanning 478 nm, from 1510 to 1988 nm. Notably, the glass achieves positive optical gain with a low population inversion threshold ($P > 0.2$), highlighting its efficiency and low-power consumption. The high glass transition temperature ($T_g \sim 842$°C) and large temperature difference ($\Delta T \sim 120$°C) between T_g and the onset of crystallization (T_x) indicate excellent thermal stability, which is crucial for producing high-quality amorphous films for on-chip amplifiers. This research examines the unique energy levels and spectral properties of the Er^{3+}-Yb^{3+}-Tm^{3+} tri-doped glass, assessing its potential for use in ultrawideband on-chip optical waveguide amplifiers. This work lays the groundwork for low-power, ultrabroadband on-chip waveguide amplifiers, offering new avenues for short-range optical interconnect systems.

Keywords: optical waveguide amplifier; low-power-consumption; ultrawideband; host material.

Received May 24, 2024; revised manuscript received Sep. 21, 2024; accepted for publication Oct. 28, 2024; published online Nov. 18, 2024.

[DOI: 10.1117/1.APN.3.6.066013]

1 Introduction

As mobile communication devices proliferate and industries, such as artificial intelligence and big data rapidly expand, optical communication systems have seen a significant surge in capacity. This has necessitated the use of various multiplexing technologies to boost the transmission capabilities of optical networks. Wavelength division multiplexing (WDM) stands out as the most cost-effective and efficient method to enhance communication capacity without altering the existing network infrastructure. However, the operational wavelength range of WDM is constrained by the gain bandwidth of the employed optical amplifiers.[1,2] The erbium-doped fiber amplifier (EDFA) is the go-to optical amplifier in WDM systems, even though its gain bandwidth covers only a fraction of the low-loss window of standard single-mode fibers.[3] Raman fiber amplifiers, which theoretically offer a broader gain bandwidth, have not gained widespread use in WDM systems due to their higher pump power requirements, leading to substantial system power consumption.[4,5] Consequently, developing optical amplifiers that offer both wide bandwidth and low-power-consumption is critical for enhancing the transmission capacity of optical communication networks.

*Address all correspondence to Mingjie Zhang, mjzhang@jnu.edu.cn; Yuanzhi Chen, yzchen@sit.edu.cn

Moreover, with on-chip photonic devices becoming increasingly integral to everyday life, on-chip optical interconnect systems also demand amplifiers that provide both large bandwidth and low-power-consumption, similar to the requirements of broader optical communication networks. Given the successful deployment of EDFA in optical networks, it seems logical to consider the erbium-doped waveguide amplifier (EDWA) for on-chip interconnect systems. However, EDWA necessitates a higher rare-earth doping concentration ($\sim 10^{21}$ cm^{-3}) in the host material due to its compact size, which not all materials can accommodate without issues, such as devitrification or reduced ion activity due to concentration quenching.[6,7] High-concentration doping also increases the likelihood of cross-relaxation-induced upconversion luminescence, which can diminish the gain in the communication band. Thus, identifying host materials that can support high rare-earth doping levels and maintain excellent luminescence properties is a key research area for on-chip optical waveguide amplifiers. Researchers have experimented with various materials, including crystal substances, such as Er^{3+}-doped lithium niobate,[8,9] Si_3N_4,[10,11] and Y_2O_3,[12] glass materials such as silicate,[13,14] chalcogenide,[15–17] and fluoride,[18,19] and polymers, such as PMMA[20,21] and PPMA.[22] Due to their broad bandwidth, isotropic properties, ease of fabrication, and superior thermal stability, Er^{3+}-doped glasses have emerged as the preferred host materials for on-chip optical waveguide amplifiers. Among these glasses, amorphous Al_2O_3 is viewed as an outstanding candidate, due to its high Er^{3+} doping capacity (up to $\sim 4.9 \times 10^{21}$ cm^{-3}),[23,24] extensive transparent window from ultraviolet (UV) to mid-infrared (150 to 5500 nm), and minimal optical loss [(0.04 ± 0.02) dB/cm in C-band].[25] Furthermore, Al_2O_3 can be readily deposited on wafers using various techniques[26–30] and is compatible with silicon photonics processing.

However, the relatively low refractive index of Al_2O_3 and its modest contrast with SiO_2 cladding have led to efforts to enhance its refractive index to improve light confinement and device integration in compact spaces.[31] This has been achieved by synthesizing high-concentration Er^{3+}-doped La_2O_3-Al_2O_3 glass, with the addition of La^{3+} not only increasing the refractive index but also preventing Er ion clustering and reducing concentration quenching.[32] Systematic studies indicate that this glass offers an optimal Er^{3+} doping level ($5Er_2O_3$-$44La_2O_3$-$51Al_2O_3$) and exhibits promising luminescence characteristics, making it an excellent host material for optical waveguide amplifiers. However, the challenge of upconversion luminescence consuming a significant portion of the pump power remains, as evidenced by the high pump threshold in the C-band. To address this, Er^{3+}-Yb^{3+} co-doped La_2O_3-Al_2O_3 glass has been developed, leveraging Yb^{3+}'s larger absorption cross section to reduce power consumption significantly. Despite these advancements, the gain bandwidth of Er^{3+}-Yb^{3+} co-doped glass remains narrow, a limitation dictated by the electronic configuration of Er^{3+} ions.

To broaden the gain bandwidth further, Er^{3+}-Yb^{3+}-Tm^{3+} tri-doped La_2O_3-Al_2O_3 glass has been designed and synthesized. The introduction of Tm^{3+} is strategic, as it offers two prominent near-infrared (NIR) emission bands that, combined with Er^{3+}'s emissions, are expected to yield an ultrawide gain bandwidth. This work establishes a foundation for the development of low-power, ultrabroadband on-chip waveguide amplifiers, presenting new opportunities for advancing short-range optical interconnect systems.

2 Materials and Methods

Glasses triply doped with Er^{3+}, Yb^{3+}, and Tm^{3+} in the composition $5Er_2O_3$-$5Yb_2O_3$-xTm_2O_3-$(44\text{-}x)La_2O_3$-$46Al_2O_3$ ($x = 0$, 0.2, 0.4, 0.6, 1, 2) were synthesized using the aerodynamic levitation (ADL) technique. The precursor materials, Er_2O_3, Yb_2O_3, Tm_2O_3, La_2O_3, and Al_2O_3, all of high purity (99.99%), were measured and mixed according to the stoichiometric ratios of the desired glass composition. The mixed oxides were then pressed into pellets ~10 mm in diameter and ~2 mm thick. These pellets were sintered into a glass phase in a muffle furnace at 1650°C and subsequently quenched at 1800°C using ADL technology. Further details on the preparation process are available in our previously published works.[6,32–34] The optical properties of the glasses were characterized using a UV-Vis-NIR spectrometer (Lambda 950, PerkinElmer, Waltham, Massachusetts) for absorption spectra and a fluorescence spectrophotometer (FLS1000, Edinburgh, United Kingdom) for emission spectra. The glass transition temperature (T_g) was determined with a differential scanning calorimeter (STA 449 F3, Netzsch).

3 Results and Discussion

Figure 1 presents the schematic of the proposed low-power-consumption, ultrawideband on-chip optical waveguide amplifier. The active region of the amplifier utilizes the newly developed and synthesized Er^{3+}-Yb^{3+}-Tm^{3+} tri-doped La_2O_3-Al_2O_3 glass. This glass outperforms the previously favored rare-earth-doped Al_2O_3 as a host material for on-chip optical waveguide amplifiers due to its higher refractive index, attributed to the high content of lanthanide elements with larger relative atomic masses. The increased refractive index enhances the waveguide's light-confinement capabilities, enabling the integration of longer waveguides within the compact chip dimensions, thereby facilitating higher gain.

The incorporation of Yb^{3+} ions, which exhibit strong absorption at the commercially available 980 nm laser wavelength, allows the waveguide amplifier to achieve efficient absorption and utilization of the pump light. This results in high gain with low pump power, epitomizing the low-power-consumption design goal. Furthermore, the co-doping with Er^{3+} and Tm^{3+} ions enable NIR broadband luminescence, with Er^{3+} and Tm^{3+} known for their excellent luminescence ~1535 and ~1860 nm, respectively. Consequently, the optical waveguide amplifier designed with Er^{3+}-Yb^{3+}-Tm^{3+} tri-doped La_2O_3-Al_2O_3 glass is expected to deliver ultrawideband NIR gain with minimal power requirements.

Figure 2(a) displays a photograph of the Er^{3+}-Yb^{3+}-Tm^{3+} tri-doped La_2O_3-Al_2O_3 glass samples, all of which appear crystal clear without any visible scattering that would indicate crystallization. This clarity suggests that the rapid cooling facilitated by the ADL technology was effective in converting all the samples into a glassy state.

As depicted in Fig. 2(b), the absorption spectra of the samples were analyzed. It is well established that the intensities of the absorption peaks at ~525, 550, 660, and 1535 nm, corresponding to the transitions of Er^{3+} from the $^4I_{15/2}$ ground state to the $^2H_{11/2}$, $^4S_{3/2}$, $^4F_{9/2}$, and $^4I_{13/2}$ excited states, respectively, remain relatively unchanged. This is attributed to the consistent Er_2O_3 content across the samples. Similarly, the absorption peak at around 980 nm, associated with the transitions Er^{3+}:$^4I_{15/2} \rightarrow {}^4I_{11/2}$ and Yb^{3+}:$^2F_{7/2} \rightarrow {}^2F_{5/2}$, shows no significant variation

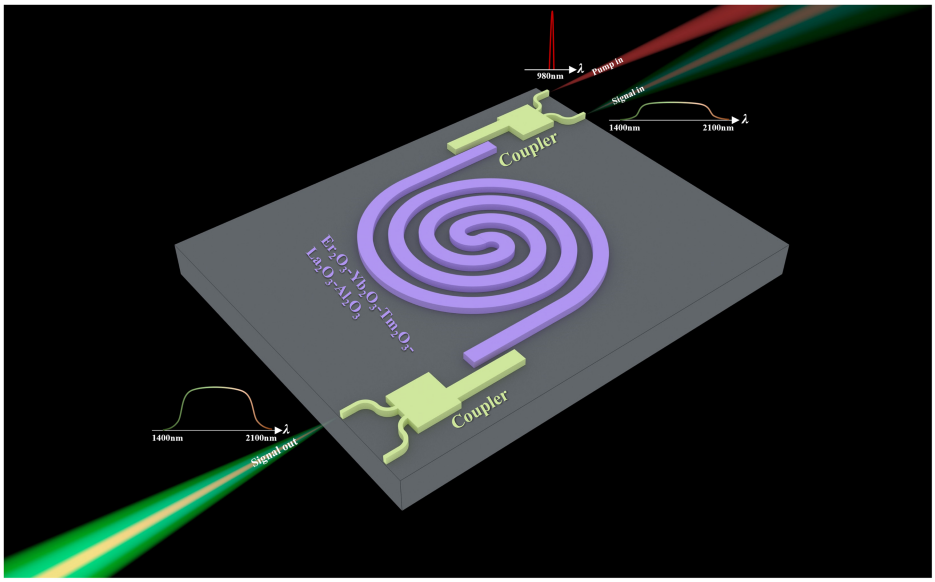

Fig. 1 3D schematic diagram of a low-power-consumption ultrawideband on-chip optical waveguide amplifier based on Er^{3+}-Yb^{3+}-Tm^{3+} tri-doped La_2O_3-Al_2O_3 glass.

in intensity due to the constant Yb_2O_3 content, mirroring the stability of the Er_2O_3 content.

In contrast, the absorption peak at ~1211 nm, which is solely attributed to the Tm^{3+}: $^3F_4 \rightarrow {}^3H_5$ transition, exhibits a gradual increase in intensity with the rising content of Tm_2O_3. The behavior of these characteristic peaks indicates that the samples possess a high degree of compositional accuracy. Further insights into the transitions of Er^{3+}, Yb^{3+}, and Tm^{3+} ions, their implications will be discussed subsequently.

The photoluminescence spectra of the glasses with the composition $5Er_2O_3$-$5Yb_2O_3$-xTm_2O_3-$(44\text{-}x)La_2O_3$-$46Al_2O_3$, where x varies from 0 to 2, were recorded under excitation with a 980 nm laser (refer to Fig. 3). Pronounced luminescence peaks are observed in both the upconversion spectra, ranging from 400 to 900 nm, and the downconversion spectra, spanning 2500 to 3000 nm [as shown in Figs. 3(a) and 3(b)]. These peaks correspond to the transitions of Er^{3+}: $^2H_{11/2} \rightarrow {}^4I_{15/2}$, $^4S_{3/2} \rightarrow {}^4I_{15/2}$, $^4F_{9/2} \rightarrow {}^4I_{15/2}$, $^4I_{9/2} \rightarrow {}^4I_{15/2}$, and $^4I_{11/2} \rightarrow {}^4I_{13/2}$, manifesting as luminescence at ~525, 550, 660, 808, and 2700 nm. These luminescence peaks correlate with the absorption peaks identified in Fig. 2(b). Notably, the intensity of the peaks at ~660 and ~2700 nm, which are typically of high intensity, exhibit a significant reduction upon the introduction of Tm_2O_3. Given that these wavelengths are not associated with Tm^{3+} transitions, the marked decrease in luminescence intensity with increasing Tm_2O_3 content suggests the presence of intricate energy transfer (ET) processes between Er^{3+} and Tm^{3+} ions. These processes will be further elucidated later in the text.

Moreover, it is important to highlight that the observed diminishment in both upconversion and downconversion luminescence intensities, particularly at ~2700 nm, contrasts with the previously reported enhancement in upconversion luminescence due to high-concentration Er^{3+} doping. The tri-doping of Er^{3+}, Yb^{3+}, and Tm^{3+} in the $La_2O_3 - Al_2O_3$ matrix leads to a concurrent weakening of both upconversion and downconversion luminescence, indicative of stronger NIR luminescence and improved pump utilization efficiency. This characteristic is highly advantageous for the development of low-power, high-gain NIR on-chip optical waveguide amplifiers.

The photoluminescence spectra of the Er^{3+}-Yb^{3+}-Tm^{3+} tri-doped La_2O_3-Al_2O_3 samples are presented in the NIR band, ranging from 1400 to 2100 nm, as shown in Fig. 3(c). As

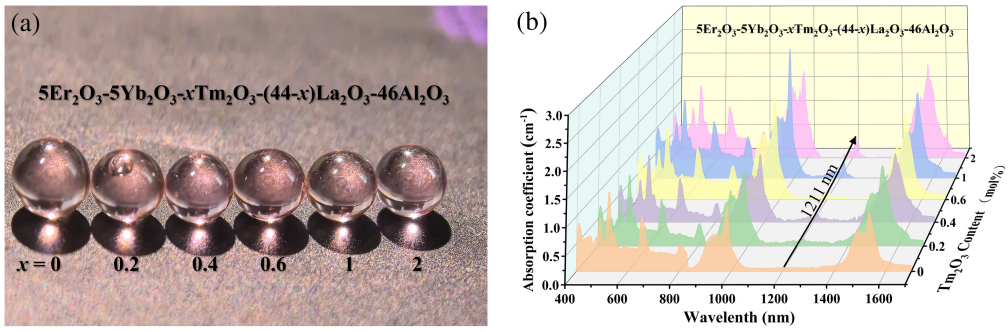

Fig. 2 (a) Photo of the $5Er_2O_3$-$5Yb_2O_3$-xTm_2O_3-$(44\text{-}x)$ La_2O_3-$46Al_2O_3$ ($x = 0, 0.2, 0.4, 0.6, 1, 2$) glass samples prepared by the ADL technique. (b) Absorption spectra of the samples in UV-Vis-NIR region.

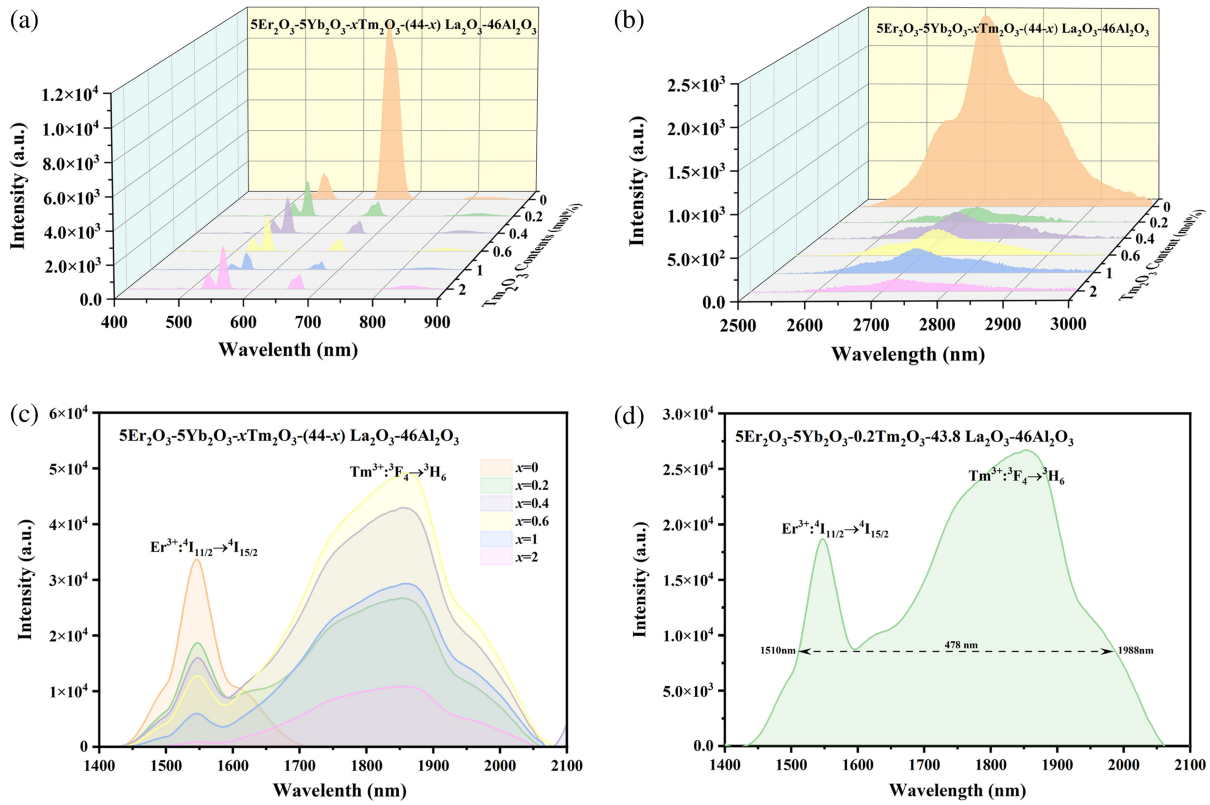

Fig. 3 Photoluminescence of $5Er_2O_3$-$5Yb_2O_3$-xTm_2O_3-$(44-x)La_2O_3$-$46Al_2O_3$ ($x = 0$, 0.2, 0.4, 0.6, 1, and 2) glasses samples under 980 nm pumping. (a) Upconversion luminescence spectra. (b) Mid-infrared luminescence spectra. (c) and (d) NIR luminescence spectra.

anticipated, the Er_2O_3-Yb_2O_3-Tm_2O_3-La_2O_3-Al_2O_3 glasses exhibit intense NIR luminescence, which is several orders of magnitude stronger than both the upconversion and downconversion luminescence around ~2700 nm. Moreover, it is evident that with increasing Tm_2O_3 content, the emission peak at ~1535 nm, attributable to the Er^{3+}:$^4I_{13/2} \rightarrow {}^4I_{15/2}$ transition, diminishes, while the emission peak at ~1860 nm, associated with the Tm^{3+}:$^3F_4 \rightarrow {}^3H_6$ transition, intensifies. This observation reinforces the presence of an ET process between Er^{3+} and Tm^{3+} ions. The interplay of these two emission peaks contributes to an ultrawide luminescence bandwidth in the NIR spectrum. Specifically, the luminescence spectrum of the glass composition $5Er_2O_3$-$5Yb_2O_3$-$0.2Tm_2O_3$-$43.8La_2O_3$-$46Al_2O_3$ spans an impressive range of ~478 nm, from ~1510 to ~1988 nm, as shown in Fig. 3(d). Furthermore, the concentrations of Er^{3+}, Yb^{3+}, and Tm^{3+} in the material are $\sim 1.56 \times 10^{21}$, $\sim 1.56 \times 10^{21}$, and $\sim 6.25 \times 10^{19}$ cm^{-3}, respectively, exhibit rare-earth ion solubility comparable to Al_2O_3, meeting the demands of matrix materials for on-chip waveguide amplifiers. This suggests that an on-chip optical waveguide amplifier based on this material could potentially offer ultrawideband gain—a feature typically achieved only with ultrahigh power pumped Raman amplifiers in the past.

The energy level diagram of Er^{3+}, Yb^{3+}, and Tm^{3+} ions is utilized to elucidate the ultrabroadband luminescence mechanism in Er^{3+}-Yb^{3+}-Tm^{3+} tri-doped La_2O_3-Al_2O_3 glasses under 980 nm laser excitation and to explicate the ET processes among these ions (refer to Fig. 4). It is well established that Yb^{3+} ions exhibit a larger absorption cross section for 980 nm light compared to Er^{3+} ions, while Tm^{3+} ions have negligible absorption at this wavelength, a characteristic dictated by the distribution of energy levels in rare-earth ions. Consequently, when Er_2O_3-Yb_2O_3-Tm_2O_3-La_2O_3-Al_2O_3 glass is pumped with a 980 nm laser, the majority of the pump photons are absorbed by Yb^{3+} ions, followed by Er^{3+} ions, with Tm^{3+} absorption being insignificant. Upon absorbing 980 nm photons, electrons in the ground state of Er^{3+}:$^4I_{15/2}$ and Yb^{3+}:$^2F_{7/2}$ are excited to the $^4I_{11/2}$ and $^2F_{5/2}$ levels, respectively. Given the short average lifetime of electrons in the Er^{3+}:$^4I_{11/2}$ excited state, they typically transition to the lower energy state $^4I_{13/2}$, emitting photons around ~2700 nm. However, achieving luminescence at ~2700 nm is challenging in practice, as the Er^{3+}:$^4I_{11/2} \rightarrow {}^4I_{13/2}$ transition is a self-terminating process that requires materials with a high Er^{3+} doping concentration, moderate phonon energy, and low OH^- concentration.[33,35] Electrons at the Er^{3+}:$^4I_{11/2}$ level usually undergo multiphonon relaxation to the $^4I_{13/2}$ level, and eventually transition to the ground state $^4I_{15/2}$, releasing photons with a wavelength of ~1535 nm. In materials with higher Er^{3+} doping concentrations, energy upconversion (ETU) and excited state absorption (ESA) processes become more probable due to the reduced distance between Er^{3+} ions. ETU and ESA lead to the excitation of more electrons to higher energy states, which, in turn, enhances upconversion luminescence due to the shorter average lifetimes of these higher excited states. This is why materials doped with high concentrations of Er^{3+} are typically more effective as hosts for upconversion luminescence.

As previously noted, Yb^{3+} ions more readily absorb pump light than Er^{3+} ions, exciting electrons from the ground state

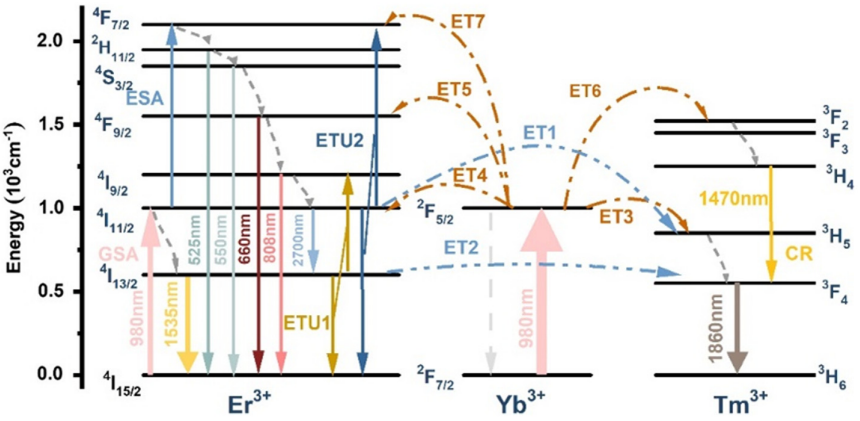

Fig. 4 Schematic diagram of the ET processes among Yb^{3+}, Er^{3+}, and Tm^{3+} in Er_2O_3-Yb_2O_3-Tm_2O_3-La_2O_3-Al_2O_3 glasses.

$^2F_{7/2}$ to the higher energy state $^2F_{5/2}$. Typically, Yb^{3+} is considered to have only these two energy levels. Within the Er^{3+}-Yb^{3+}-Tm^{3+} tri-doped La_2O_3-Al_2O_3 glass, electrons in the high energy state $^2F_{5/2}$ of Yb^{3+} transfer energy to corresponding energy levels of Er^{3+} and Tm^{3+}, leading to a reversal in the population of these levels, as shown in Fig. 4. These ETs enhance the luminescence of Er^{3+} and Tm^{3+} and improve the pump light utilization efficiency. In addition to energy being transferred from the excited Yb^{3+} ions to Tm^{3+} ions, ET also occurs between Er^{3+} and Tm^{3+}, as illustrated in the figure. Electrons in Tm^{3+}:$^3F_2$, which achieve population inversion through ET processes, transition to $3H_4$ via multiphonon relaxation, and then further transition to $^3F_4$ while emitting photons at ∼1470 nm. Along with the electrons transitioning from Tm^{3+}:$^3H_5$ to $^3F_4$ through multiphonon relaxation, electrons at this level eventually transition to the ground state $^3H_6$, emitting photons at ∼1860 nm. This explains why the Er^{3+}-Yb^{3+}-Tm^{3+} tri-doped material can emit light at ∼1470 and ∼1860 nm, even though Tm^{3+} does not absorb the 980 nm pump light. However, the photoluminescence spectra presented earlier in this article indicate a reduction in the upconversion and downconversion luminescence of Er^{3+} near ∼2700 nm, alongside an enhancement of NIR luminescence, with no significant luminescence of Tm^{3+} at ∼1470 nm being observed. This leads us to believe that, at least in the Er_2O_3-Yb_2O_3-Tm_2O_3-La_2O_3-Al_2O_3 glasses, the ET processes among Er^{3+}, Yb^{3+}, and Tm^{3+} predominantly occur among lower energy levels, such as ET1, ET2, ET3, and ET4. This is highly advantageous for achieving NIR luminescence and will greatly benefit the use of this material in low-power-consumption NIR on-chip optical waveguide amplifiers.

The Judd–Ofelt (J-O) theory is commonly employed to determine the spectral parameters of rare-earth-doped materials, which in turn are used to assess the luminescence properties of these materials. To explore the potential of $5Er_2O_3$-$5Yb_2O_3$-$0.2Tm_2O_3$-$43.8La_2O_3$-$46Al_2O_3$ glass as a host material for on-chip optical waveguide amplifiers, J-O theory is applied to calculate the transition probability (A_R) and branching ratio (β_R) of the material. Eleven absorption bands in the absorption spectrum are used to fit the transition strength parameters Ω_t ($t = 2, 4, 6$), which correspond to the optical transitions of Er^{3+} ions from the ground state $^4I_{15/2}$ to various excited states. The spectral parameters of the $5Er_2O_3$-$5Yb_2O_3$-$0.2Tm_2O_3$-$43.8La_2O_3$-$46Al_2O_3$ glass are presented and summarized in Table 1. This includes the experimental oscillator strength ($f_{exp.}$), the calculated oscillator strength ($f_{cal.}$), the experimental electric dipole line strength ($S_{exp.}$), and the calculated electric

Table 1 Experimental and calculated oscillator strength of $5Er_2O_3$-$5Yb_2O_3$-$0.2Tm_2O_3$-$43.8La_2O_3$-$46Al_2O_3$ glass.

$^4I_{15/2}$ →	λ_{start}-λ_{end} (nm)	$\bar{\lambda}$ (nm)	$f_{exp.}$ (×10^{-6})	$S_{exp.}$ (×10^{-20} cm^2)	$S_{cal.}$ (×10^{-20} cm^2)
$^4I_{13/2}$	1500 to 1680	1546	1.226	1.519	1.492
$^4I_{11/2}$	920 to 980	960	0.611	0.470	0.399
$^4I_{9/2}$	802 to 850	826	0.270	0.178	0.100
$^4F_{9/2}$	635 to 692	657	2.029	1.069	1.063
$^4S_{3/2}$	545 to 569	551	0.520	0.230	0.207
$^2H_{11/2}$	512 to 530	523	1.977	0.828	0.944
$^4F_{7/2}$	471 to 520	498	1.783	0.711	0.743
$^4F_{5/2}$	446 to 471	454	0.659	0.240	0.208
$^4F_{3/2}$	425 to 446	438	0.258	0.090	0.120
$^2H_{9/2}$	410 to 425	414	0.708	0.235	0.241
$^4H_{11/2}$	365 to 401	379	5.757	1.747	1.713

$\Omega_2 = 0.901 \times 10^{-20}$ cm^2, $\Omega_4 = 1.056 \times 10^{-20}$ cm^2, and $\Omega_6 = 0.943 \times 10^{-20}$ cm^2, $R = 5.35\%$.

dipole line strength ($S_{cal.}$). The relative square deviation between the measured and calculated electric-dipole oscillator strengths is used as a measure of the fitting quality (R), which can be expressed by

$$R = \left\{ \frac{\sum (f_{exp.} - f_{cal.})^2}{\sum f_{exp.}^2} \right\}. \quad (1)$$

This equation quantifies the discrepancy between the experimental and theoretical values, providing insight into the accuracy of the J-O theory in predicting the luminescence properties of the material in question.

The R value represents the square deviation between experimental and theoretical oscillator strengths, serving as an indicator of the fitting quality. The J-O intensity parameters (Ω_2, Ω_4, and Ω_6) for the $5Er_2O_3$-$5Yb_2O_3$-$0.2Tm_2O_3$-$43.8La_2O_3$-$46Al_2O_3$ glass are 0.901×10^{-20}, 1.056×10^{-20}, and 0.943×10^{-20} cm^2, respectively. These parameters are indicative of the local environment and the nature of bonding around the rare-earth ions. Ω_2, in particular, is highly sensitive to the local environment of rare-earth ions, reflecting the asymmetry of the coordination structure, bonding characteristics, and polarizability of the ligand ions or molecules. The relatively small value of Ω_2 for the $5Er_2O_3$-$5Yb_2O_3$-$0.2Tm_2O_3$-$43.8La_2O_3$-$46Al_2O_3$ glass suggests a higher symmetry in the coordination structure around Er^{3+} ions and denotes a high degree of material uniformity.

Radiative properties, such as the radiative transition probability (A_R), stimulated emission cross section (σ), and branching ratio (β_R) for the excited state of Er^{3+} are calculated based on the J-O parameters previously obtained and are summarized in Table 2. For the detailed calculation equations, readers are referred to the literature.[36–38]

Compared to the A_R of $5Er_2O_3$-$44La_2O_3$-$51Al_2O_3$ glass (125.46 s^{-1}), the A_R of $5Er_2O_3$-$5Yb_2O_3$-$0.2Tm_2O_3$-$43.8La_2O_3$-$46Al_2O_3$ glass (173.74 s^{-1}) for the $^4I_{13/2} \rightarrow {}^4I_{15/2}$ transition is higher. This suggests that the incorporation of Yb^{3+} and Tm^{3+} enhances the luminescence in the NIR band. Furthermore, the branching ratio β_R for the $^4I_{11/2} \rightarrow {}^4I_{13/2}$ transition is 21.3%, which is lower than that of the $5Er_2O_3$-$44La_2O_3$-$51Al_2O_3$ glass. This indicates that the introduction of Yb^{3+} and Tm^{3+} leads to a decrease in luminescence at ~2700 nm, a finding corroborated by the photoluminescence spectrum presented earlier in this article. This also reflects the accuracy of the parameters calculated using J-O theory and the potential for low power consumption when using this material to achieve NIR luminescence.

To further verify the low-power-consumption characteristics of the $5Er_2O_3$-$5Yb_2O_3$-$0.2Tm_2O_3$-$43.8La_2O_3$-$46Al_2O_3$ glass in the ultrawideband NIR band, the absorption and emission cross-sections around ~1535 and ~1860 nm were calculated for the transitions $Er^{3+}:{}^4I_{13/2} \rightarrow {}^4I_{15/2}$ and $Tm^{3+}:{}^3F_4 \rightarrow {}^3H_6$, respectively. The absorption cross section (σ_{abs}) is determined from the measured absorption spectrum using the Beer–Lambert law, as given by

$$\sigma_{abs}(\lambda) = \frac{\alpha(\lambda)}{N}, \quad (2)$$

Table 2 Spectral parameters of $5Er_2O_3$-$5Yb_2O_3$-$0.2Tm_2O_3$-$43.8La_2O_3$-$46Al_2O_3$ glass for the radiative transition.

Transition					
Initial state	Final state	Radiation λ (nm)	Transition probability A_R (s^{-1})	Branch ratio β_R (%)	Lifetime $\tau/\mu s$
$^4I_{13/2}$	$^4I_{15/2}$	1636	173.74	100	5756
$^4I_{11/2}$	$^4I_{15/2}$	1022	149.90	78.70	4886
	$^4I_{13/2}$	2721	40.56	21.30	
$^4I_{9/2}$	$^4I_{15/2}$	817	87.61	54.50	5251
	$^4I_{13/2}$	1633	67.28	41.86	
	$^4I_{11/2}$	4082	5.85	3.64	
$^4F_{9/2}$	$^4I_{15/2}$	638	1964.61	88.34	450
	$^4I_{13/2}$	1047	126.70	5.70	
	$^4I_{11/2}$	1701	125.10	5.63	
	$^4I_{9/2}$	2917	7.49	0.34	
$^4S_{3/2}$	$^4I_{15/2}$	527	1693.53	62.57	369
	$^4I_{13/2}$	778	819.36	30.27	
	$^4I_{11/2}$	1089	68.63	2.54	
	$^4I_{9/2}$	1486	124.79	4.61	
	$^4F_{9/2}$	3027	0.35	0.01	
$^2H_{11/2}$	$^4I_{15/2}$	522	2657.87	87.52	329
	$^4I_{13/2}$	767	235.07	7.74	
	$^4I_{11/2}$	1067	78.94	2.6	
	$^4I_{9/2}$	1445	58.72	1.93	
	$^4F_{9/2}$	2864	6.30	0.21	
	$^4S_{3/2}$	53,402	0.0005	0	

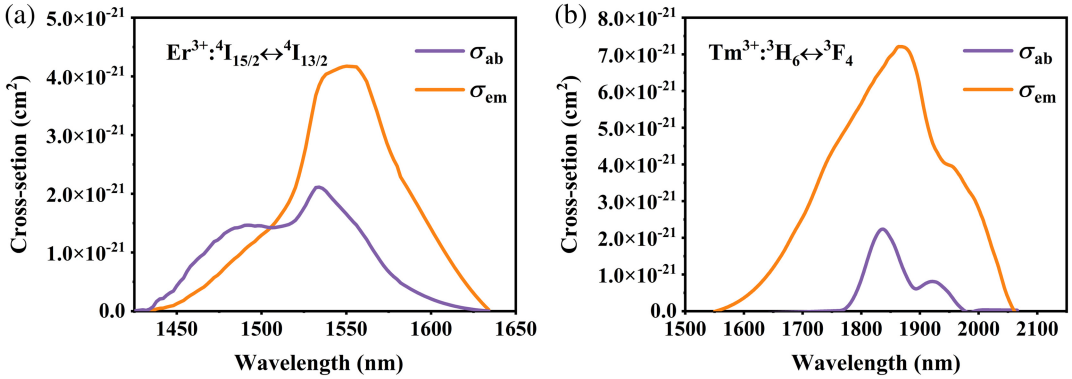

Fig. 5 Absorption and emission cross sections of (a) $Er^{3+}:{}^4I_{15/2}\leftrightarrow{}^4I_{13/2}$ transitions and (b) $Tm^{3+}:{}^3H_6\leftrightarrow{}^3F_4$ transitions.

where $\alpha(\lambda)$ is the absorption coefficient at wavelength λ. The emission cross section (σ_{em}) is determined using the Fuchtbauer–Ladenburg (F-L) model, as given by

$$\sigma_{em}(\lambda)=\frac{\lambda^4 A_{rad}}{8\pi c n^2}\frac{\lambda I(\lambda)}{\int \lambda I(\lambda)\mathrm{d}\lambda}, \tag{3}$$

where A_{rad} is the radiative transition probability, n is the refractive index, and $I(\lambda)$ is the measured fluorescence emission intensity at wavelength λ. The calculated absorption and emission cross sections are shown below.

The calculated absorption and emission cross sections clearly indicate that the emission cross sections near ~1535 and ~1860 nm are substantially larger than the absorption cross sections, as shown in Figs. 5(a) and 5(b), suggesting the potential for significant gains within these bands. Moreover, by integrating the obtained emission and absorption cross sections, the gain cross section for the $5Er_2O_3$-$5Yb_2O_3$-$0.2Tm_2O_3$-$43.8La_2O_3$-$46Al_2O_3$ glass was calculated by

$$G(\lambda)=P\cdot\sigma_{em}(\lambda)-(1-P)\cdot\sigma_{abs}(\lambda). \tag{4}$$

Here, P represents the population inversion of Er^{3+} or Tm^{3+}, defined as $P=N_2/(N_2+N_1)$, where N_1 and N_2 are the population densities of the ground and excited states, respectively. The gain spectra around ~1535 and ~1860 nm for the $5Er_2O_3$-$5Yb_2O_3$-$0.2Tm_2O_3$-$43.8La_2O_3$-$46Al_2O_3$ glass, as depicted in Fig. 6, show that as P increases, the bandwidth encompassed by the positive gain spectrum also expands. It is evident from the results that the gain transitions from negative to positive as P rises. A positive gain is achievable in both spectral bands when $P>0.2$, indicating that minimal pump power is required to achieve gain, thus confirming the material's low power consumption. Notably, as the positive gain intensifies, its bandwidth correspondingly broadens. These spectral properties unequivocally establish that the $55Er_2O_3$-$5Yb_2O_3$-$0.2Tm_2O_3$-$43.8La_2O_3$-$46Al_2O_3$ glass possesses characteristics of low power consumption and ultrawideband gain, making it an exemplary host material for the energy-efficient, ultrawideband, on-chip optical waveguide amplifiers.

For a host material to be suitable for low-power-consumption ultrawideband on-chip optical waveguide amplifiers, it must exhibit not only exceptional spectral characteristics but also outstanding thermal stability, especially since high-power lasers will be confined within a material of limited size. To this end, we analyzed the thermal properties of the $55Er_2O_3$-$5Yb_2O_3$-$0.2Tm_2O_3$-$43.8La_2O_3$-$46Al_2O_3$ glass using differential scanning calorimetry (DSC). The DSC curve, obtained at a heating rate of 20°C/min and depicted in Fig. 7, reveals the glass transition temperature (T_g) and the onset crystallization temperature (T_x) to be ~842°C and 962°C, respectively.

When compared to current contenders for on-chip optical waveguide amplifiers, such as silicate, tellurite, fluoride, chalcogenide glasses, and polymers, the high T_g of the $55Er_2O_3$-$5Yb_2O_3$-$0.2Tm_2O_3$-$43.8La_2O_3$-$46Al_2O_3$ glass suggests superior thermal stability. Furthermore, the difference between

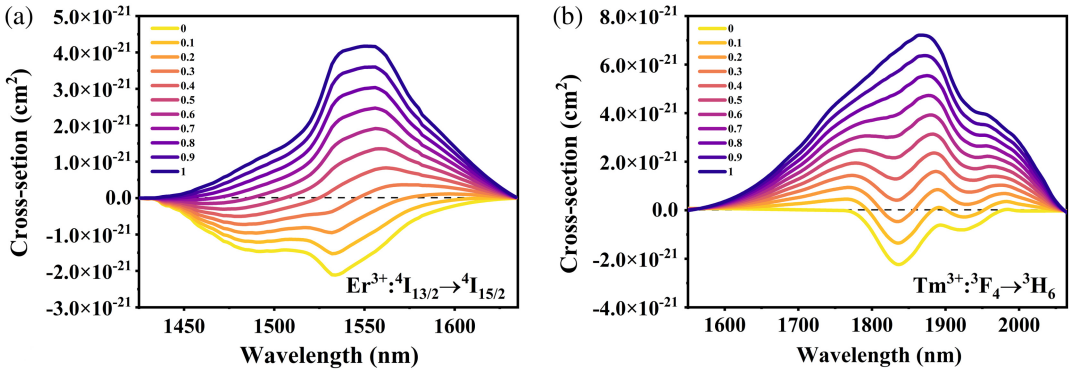

Fig. 6 Gain cross sections of (a) $Er^{3+}:{}^4I_{13/2}\rightarrow{}^4I_{15/2}$ transitions and (b) $Tm^{3+}:{}^3F_4\rightarrow{}^3H_6$ transitions.

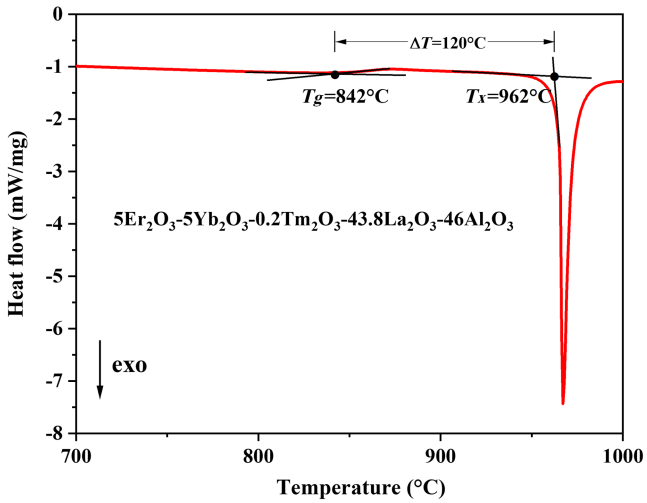

Fig. 7 (a) DSC curves of $5Er_2O_3$-$5Yb_2O_3$-$0.2Tm_2O_3$-$43.8La_2O_3$-$46Al_2O_3$ glass at a heating rate of 20°C/min.

T_x and T_g, denoted as ΔT, is commonly used to assess a material's glass-forming ability. With a ΔT of 120°C, this glass demonstrates robust thermal resistance to crystallization. This characteristic provides a solid foundation for the fabrication of high-quality amorphous films of $55Er_2O_3$-$5Yb_2O_3$-$0.2Tm_2O_3$-$43.8La_2O_3$-$46Al_2O_3$, which are essential for on-chip optical waveguide amplifiers. In general, producing thin films with uniform elemental distribution, akin to bulk materials, is challenging. However, a larger ΔT expands the temperature window for deposition techniques such as single-target magnetron sputtering, pulsed laser deposition (LPD), multitarget magnetron sputtering, and atomic layer deposition (ALD), thereby enabling the fabrication of high-quality multicomponent amorphous films. In addition, the elevated T_g, T_x, and larger ΔT offer enhanced thermal stability during high-temperature annealing, facilitating the conversion of rare-earth metals into rare-earth ions. This process activates the absorption and emission of Er^{3+}, Yb^{3+}, and Tm^{3+}, bringing the luminescent properties of the films and waveguides closer to those of their bulk counterparts.[39–41]

The superior luminescence properties and thermal stability of the $55Er_2O_3$-$5Yb_2O_3$-$0.2Tm_2O_3$-$43.8La_2O_3$-$46Al_2O_3$ glass, as demonstrated in our study, unequivocally establish it as an ideal host material for low-power-consumption, ultrawideband on-chip optical waveguide amplifiers. This glass composition, enriched with lanthanide elements that have larger relative atomic masses compared to rare-earth-doped Al_2O_3, results in a higher refractive index. This property is advantageous for achieving high-density integration within the confined spaces of on-chip environments, as illustrated in Fig. 1. To optimize the pump light utilization efficiency, the ridge waveguide depicted in Fig. 1 was meticulously designed using COMSOL Multiphysics. The resulting waveguide dimensions are 1000 nm in width and 6000 nm in height, as shown in Fig. 8. The structural optimization took into account the confinement factors (Γ) of both the pump and signal lights for the spectral bands around ∼1535 and ∼1860 nm. According to the definition by Robinson et al., the confinement factor Γ for a given mode in the active region S of a high-index contrast waveguide is given by[42]

$$\Gamma = \frac{n_{\text{eff}}^{g}}{n_{S}^{g}} \frac{\iint_{0}^{S} \epsilon |E(x,y)|^2 \mathrm{d}x\,\mathrm{d}y}{\iint_{-\infty}^{+\infty} \epsilon |E(x,y)|^2 \mathrm{d}x\,\mathrm{d}y}. \tag{5}$$

In this equation, n_{eff}^{g} is the effective group index of the mode, n_{S}^{g} is the group index of the active region S, ϵ is the permittivity of the waveguide host material, and $E(x,y)$ represents the electric field distribution of the mode for the given cross section. Our calculations determined the confinement factors Γ for the fundamental TE-mode pump beam at 980 nm and the signal beams at 1535 and 1860 nm. The electric field distributions at these three wavelengths are depicted in the corresponding figure, yielding confinement factors of $\Gamma_{980\text{ nm}} \approx 0.92$, $\Gamma_{1535\text{ nm}} \approx 0.77$, and $\Gamma_{1860\text{ nm}} \approx 0.65$. A higher Γ value indicates a greater overlap between the beam (pump and signal) and the active area of the waveguide, facilitating more rare-earth ions to

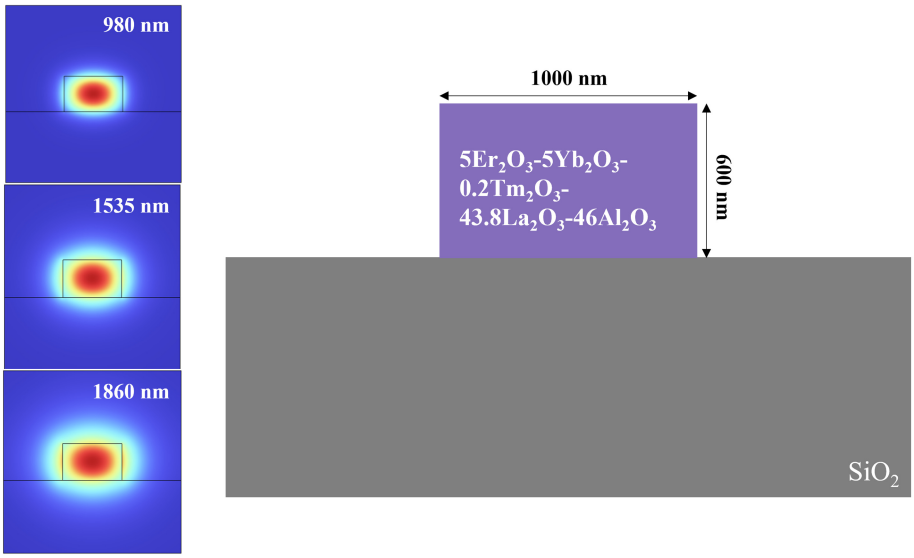

Fig. 8 $5Er_2O_3$-$5Yb_2O_3$-$0.2Tm_2O_3$-$43.8La_2O_3$-$46Al_2O_3$ ridge waveguide and the electric field distributions of TE modes at 980, 1535, and 1860 nm.

engage in the pump absorption and signal amplification processes. Consequently, we posit that on-chip optical amplifiers based on the $55Er_2O_3$-$5Yb_2O_3$-$0.2Tm_2O_3$-$43.8La_2O_3$-$46Al_2O_3$ glass are capable of achieving low-power-consumption, ultrawideband gain.

4 Conclusion

A suite of high-concentration Er^{3+}-Yb^{3+}-Tm^{3+} tri-doped La_2O_3-Al_2O_3 glasses, intended for use as host materials in on-chip optical waveguide amplifiers, were synthesized via ADL technology. The incorporation of Tm_2O_3 led to a marked reduction in both upconversion and downconversion luminescence intensities around ∼2700 nm. This reduction resulted in a pronounced enhancement of the glasses' luminescence intensity within the NIR band, exhibiting an intensity 3 orders of magnitude greater than that of other bands. Furthermore, the NIR luminescence spectrum of the $55Er_2O_3$-$5Yb_2O_3$-$0.2Tm_2O_3$-$43.8La_2O_3$-$46Al_2O_3$ glass spans a broad range from ∼1510 to 1988 nm, covering up to 478 nm. Calculations of absorption, emission, and gain cross sections reveal that the glass can achieve positive gain with a population inversion $P > 0.2$, indicating that only low pump power is required for positive gain, thus highlighting its low-power-consumption attribute. The high glass transition temperature (T_g) of ∼842°C and a significant ΔT of ∼120°C suggest outstanding thermal stability and facilitate the preparation of amorphous thin films. The combination of low pump power requirements, extensive bandwidth, superior thermal stability, and favorable glass-forming capabilities confirms that the $55Er_2O_3$-$5Yb_2O_3$-$0.2Tm_2O_3$-$43.8La_2O_3$-$46Al_2O_3$ glass is an exemplary host material for energy-efficient, ultrawideband on-chip optical waveguide amplifiers. This will facilitate the development and application of low-power, ultrabroadband on-chip waveguide amplifiers, providing new options for the advancement of short-range optical interconnect systems.

Disclosures

The authors declare no conflicts of interest.

Code and Data Availability

Data underlying the results in this paper may be obtained from the authors upon reasonable request.

Acknowledgments

This work was supported by the National Natural Science Foundation of China (Grant No. 62005098), the Fundamental Research Funds for the Central University (Grant No. 11623415), and the Guangzhou Science and Technology Planning Project (Grant No. 202201010320).

References

1. Y. Fu et al., "(S+C)-band polymer waveguide amplifier based on Tm^{3+} and Er^{3+} layer-doped core-shell nanoparticles," *Opt. Lett.* **48**(2), 391–394 (2023).
2. J. Clark and G. Lanzani, "Organic photonics for communications," *Nat. Photonics* **4**(7), 438–446 (2010).
3. H. Chen et al., "Integrated cladding-pumped multicore few-mode erbium-doped fibre amplifier for space-division-multiplexed communications," *Nat. Photonics* **10**(8), 529–533 (2016).
4. H. Ying et al., "Raman-noise enhanced stimulated Raman scattering in high-power continuous-wave fiber amplifier," *Optik* **144**, 163–171 (2017).
5. L. Sirleto and M. A. Ferrara, "Fiber amplifiers and fiber lasers based on stimulated Raman scattering: a review," *Micromachines (Basel)* **11**(3), 247 (2020).
6. S. Huang et al., "Luminescent properties of Er^{3+}-doped La_2O_3-Ga_2O_3 glass prepared by aerodynamic levitation technique," *J. Lumin.* **239**, 118355 (2021).
7. B. Singarapu et al., "Glass-ceramics processed by spark plasma sintering (SPS) for optical applications," *Appl. Sci.* **10**(8), 2791 (2020).
8. Z. Chen et al., "Efficient erbium-doped thin-film lithium niobate waveguide amplifiers," *Opt. Lett.* **46**(5), 1161–1164 (2021).
9. J. Zhou et al., "On-chip integrated waveguide amplifiers on erbium-doped thin–film lithium niobate on insulator," *Laser Photon. Rev.* **15**(8), 2100030 (2021).
10. J. Mu et al., "High-gain waveguide amplifiers in Si_3N_4 technology via double-layer monolithic integration," *Photonics Res.* **8**(10), 1634–1641 (2020).
11. J. Rönn et al., "Erbium-doped hybrid waveguide amplifiers with net optical gain on a fully industrial 300 mm silicon nitride photonic platform," *Opt. Express* **28**(19), 27919–27926 (2020).
12. E. Lizarraga-Medina et al., "Al_2O_3-Y_2O_3 nanolaminated slab optical waveguides by atomic layer deposition," *Opt. Mater.* **103**, 109822 (2020).
13. F. Ondracek et al., "Er-Yb waveguide amplifiers in novel silicate glasses," *IEEE J. Quantum Electron.* **44**(6), 536–541 (2008).
14. J. Šmejcký et al., "Erbium-bismuth-doped germanium silicate active optic glass for broad-band optical amplification," *Opt. Mater.* **137**, 113621 (2023).
15. K. Yan et al., "Greater than 50% inversion in erbium doped chalcogenide waveguides," *Opt. Express* **24**(20), 23304–23313 (2016).
16. K. Yan, K. Vu, and S. Madden, "Internal gain in Er-doped As_2S_3 chalcogenide planar waveguides," *Opt. Lett.* **40**(5), 796–799 (2015).
17. C. Wang et al., "High-gain waveguide amplifiers in $Ge_{25}Sb_{10}S_{65}$ photonics heterogeneous integration with erbium-doped Al_2O_3 thin films," *Laser Photonics Rev.* **18**(3), 2300893 (2024).
18. B. Boulard, "Fluoride glasses and planar optical waveguides," *Functionalized Inorganic Fluorides* **11**, 331 (2010).
19. J. D. Bradley and M. Pollnau, "Erbium-doped integrated waveguide amplifiers and lasers," *Laser Photon. Rev.* **5**(3), 368–403 (2011).
20. X. Liu, M. Zhang, and G. Hu, "Gain enhancement of the optical waveguide amplifier based on $NaYF_4$/$NaLuF_4$: Yb, Er NPs-PMMA integrated with a Si_3N_4 slot," *Nanomaterials (Basel)* **12**(17), 2937 (2022).
21. M. Zhang et al., "High-gain polymer optical waveguide amplifiers based on core-shell $NaYF_4$/$NaLuF_4$: Yb^{3+}, Er^{3+} NPs-PMMA covalent-linking nanocomposites," *Sci. Rep.* **6**(1), 36729 (2016).
22. C. Grivas and M. Pollnau, "Organic solid-state integrated amplifiers and lasers," *Laser Photon. Rev.* **6**(4), 419–462 (2012).
23. J. Rönn et al., "Ultra-high on-chip optical gain in erbium-based hybrid slot waveguides," *Nat. Commun.* **10**(1), 1–9 (2019).
24. P. Xiao and B. Wang, "Design of an erbium-doped Al_2O_3 optical waveguide amplifier with on-chip integrated laser pumping source," *Opt. Commun.* **508**, 127709 (2022).
25. M. Demirtaş et al., "Low loss atomic layer deposited Al_2O_3 waveguides for applications in on-chip optical amplifiers," *IEEE J. Sel. Top. Quantum Electronics* **24**(4), 1–8 (2018).
26. R. Serna et al., "Enhanced photoluminescence of rare-earth doped films prepared by off-axis pulsed laser deposition," *Appl. Surf. Sci.* **257**(12), 5204–5207 (2011).
27. G. Balakrishnan et al., "Growth of highly oriented γ-and α-Al_2O_3 thin films by pulsed laser deposition," *Opt. Laser Technol.* **56**, 317–321 (2014).
28. R. Takakura et al., "Room-temperature bonding of Al_2O_3 thin films deposited using atomic layer deposition," *Sci. Rep.* **13**(1), 3581 (2023).

29. X. Chen et al., "Rational selection of the oxygen source for atomic layer deposition Al_2O_3 insulators," *Vacuum* **215**, 112315 (2023).
30. J. Yu et al., "Recent advances on pulsed laser deposition of large-scale thin films," *Small Methods* **8**(7), 2301282 (2024).
31. Z. Su et al., "High-Q-factor Al_2O_3 micro-trench cavities integrated with silicon nitride waveguides on silicon," *Opt. Express* **26**(9), 11161–11170 (2018).
32. C. Wang et al., "Synthesis and study of novel erbium-doped La_2O_3-Al_2O_3 glasses for on-chip waveguide amplifier," *J. Alloys Compd.* **899**, 162915 (2022).
33. M. Zhang et al., "Study on Er^{3+}-Yb^{3+} co-doped La_2O_3-Al_2O_3 glasses for C-band optical waveguide amplifier with high luminous efficiency and low pump threshold," *Ceram. Int.* **48**(21), 32236–32240 (2022).
34. Y. Chen et al., "High content Er^{3+}-doped $25La_2O_3$-$75Ga_2O_3$ glass: a potential material for high-power lasers or EDWA," *J. Alloys Compd.* **837**, **155477** (2020).
35. K. Yoshimoto et al., "2.7 μm mid-infrared emission in highly erbium-doped lanthanum gallate glasses prepared via an aerodynamic levitation technique," *Adv. Opt. Mater.* **6**(8), 1701283 (2018).
36. G. S. Ofelt, "Intensities of crystal spectra of rare-earth ions," *J. Chem. Phys.* **37**(3), 511–520 (1962).
37. B. R. Judd, "Optical absorption intensities of rare-earth ions," *Phys. Rev.* **127**(3), 750–761 (1962).
38. Y. Shao et al., "Growth and spectroscopic properties investigation of Er-doped BGSO single crystal: a potential gain medium for eye-safe laser," *Ceram. Int.* **49**(11), 17534–17541 (2023).
39. R. Liu et al., "Erbium-doped Ga_2O_3 waveguide for optical amplification," *Appl. Phys. Lett.* **123**(15) (2023).
40. Z. Zhang et al., "On-chip Er-doped Ta_2O_5 waveguide amplifiers with a high internal net gain," *Opt. Lett.* **48**(21), 5799–5802 (2023).
41. W. Wang et al., "Origin of thermally activated Er^{3+} emission in GeGaSe films and waveguides," *Opt. Lett.* **48**(21), 5715–5718 (2023).
42. J. T. Robinson et al., "First-principle derivation of gain in high-index-contrast waveguides," *Opt. Express* **16**(21), 16659–16669 (2008).

Biographies of the authors are not available.